International Immunology, Vol. 33, No. 11, pp. 587–594
https://doi.org/10.1093/intimm/dxab060
Advance Access publication 29 August 2021

Using a new three-dimensional CUBIC tissue-clearing method to examine the brain during experimental cerebral malaria

Julia Matsuo-Dapaah[1,2], Michelle Sue Jann Lee[1], Ken J. Ishii[2,3,4,5], Kazuki Tainaka[6,7] and Cevayir Coban[1,2,4,5]

[1]Division of Malaria Immunology, Department of Microbiology and Immunology, Institute of Medical Science (IMSUT), University of Tokyo, Tokyo 108-8639, Japan
[2]Graduate School of Medicine, University of Tokyo, Tokyo 113-8654, Japan
[3]Division of Vaccine Science, Department of Microbiology and Immunology, Institute of Medical Science (IMSUT), University of Tokyo, Tokyo 108-8639, Japan
[4]International Vaccine Design Center, Institute of Medical Science (IMSUT), University of Tokyo, Tokyo 108-8639, Japan
[5]Immunology Frontier Research Center (IFReC), Osaka University, Osaka 565-0871, Japan
[6]Department of System Pathology for Neurological Disorders, Center for Bioresources, Brain Research Institute, Niigata University, Niigata 951-8585, Japan
[7]Laboratory for Synthetic Biology, RIKEN Center for Biosystems Dynamics Research, Osaka 565-0871, Japan

Correspondence to: C. Coban; E-mail: ccoban@ims.u-tokyo.ac.jp or K. Tainaka; E-mail: kztainaka@bri.niigata-u.ac.jp

Received 30 April 2021, *editorial decision* 27 August 2021; *accepted* 28 August 2021

Abstract

Cerebral malaria (CM) is a life-threatening complication of the malaria disease caused by *Plasmodium falciparum* infection and is responsible for the death of half a million people annually. The molecular pathogenesis underlying CM in humans is not completely understood, although sequestration of infected erythrocytes in cerebral microvessels is thought to play a major role. In contrast, experimental cerebral malaria (ECM) models in mice have been thought to be distinct from human CM, and are mainly caused by inflammatory mediators. Here, to understand the spatial distribution and the potential sequestration of parasites in the whole-brain microvessels during a mouse model of ECM, we utilized the new tissue-clearing method CUBIC (Clear, Unobstructed, Brain/Body Imaging Cocktails and Computational analysis) with light-sheet fluorescent microscopy (LSFM), and reconstructed images in three dimensions (3D). We demonstrated significantly greater accumulation of *Plasmodium berghei* ANKA (*Pb*ANKA) parasites in the olfactory bulb (OB) of mice, compared with the other parts of the brain, including the cerebral cortex, cerebellum and brainstem. Furthermore, we show that *Pb*ANKA parasites preferentially accumulate in the brainstem when the OB is surgically removed. This study therefore not only highlights a successful application of CUBIC tissue-clearing technology to visualize the whole brain and its microvessels during ECM, but it also shows CUBIC's future potential for visualizing pathological events in the whole ECM brain at the cellular level, an achievement that would greatly advance our understanding of human cerebral malaria.

Keywords: α-SMA, brainstem, bulbectomy, olfactory bulb, *Plasmodium berghei*

Introduction

Malaria is a global burden affecting millions of people and causing half a million deaths each year, mainly due to its unique complication in the brain called cerebral malaria (1). The brain is severely disrupted by *Plasmodium falciparum* infection in man (human cerebral malaria, HCM), and by *Plasmodium berghei* ANKA (*Pb*ANKA) infection in mice (experimental cerebral malaria, ECM). In humans, the presence of mostly ring-stage-infected erythrocytes in the peripheral blood and the sequestration of late-stage parasites in the brain (seen post-mortem) have been considered as the main cause for the initiation of HCM, with less attention paid to the role of inflammation and immune cell activation (2). In contrast, several studies in mice have focussed on the role of inflammation and immune system-mediated ECM pathology

in the brain, such as the activation of $CD8^+$ T cells, microglia and astrocytes which may eventually lead to blood–brain barrier (BBB) disruption, oedema and pathology (3). Notably, the differences between HCM and ECM have been diminishing with the recent emerging studies focussing on the wide range of similarities between the mouse and human forms, including the accumulation and occlusion of infected red blood cells (iRBC) in the mouse brain and the accumulation of $CD8^+$ T cells in the human brain (for more information readers are referred to the recent excellent review articles (2–4)). However, comprehensive understanding of how an obligate erythrocyte-resident pathogen circulating in the blood vessels can cause pathology in the brain at present remains elusive.

Recent imaging technologies in pre-clinical studies in our laboratory using ultra-high-field 11.7 T magnetic resonance imaging (MRI) and multi-photon live imaging microscopy have revealed new findings about the pathology of ECM. Accordingly, the olfactory bulb (OB) is the first region to exhibit vascular leakage and oedema during ECM (5), which later progress along the rostral migratory route to the brainstem (6–11). The OB is located on the cribriform plate over the nasal sinus and has unique vessel structures with dense trabecular blood capillaries surrounded by microglia and astrocyte end-feet (3). A key role of the dense and directionally structured olfactory blood capillaries (12) may be to act as a suitable scaffold for infected erythrocyte sequestration and inflammation, as hypothesized in our previous study; however, MRI imaging does not have adequate resolution to visualize and distinguish deep capillaries within the tissue (13). Furthermore, the multi-photon live imaging used in our previous study is a point-scanning technique that is able to visualize brain microvessels only at a limited depth and field of view (14, 15). Therefore, whole-brain imaging of deep vessels with single-microvessel quality and resolution is needed for understanding the interactions between the erythrocyte-invading *Plasmodium* parasite and brain vessels as well as tissues.

To date, several tissue-clearing methods have been developed for the purpose of robust labelling and optical imaging of deep tissues and vessel structures of the brain in both healthy and diseased conditions (13, 16). The CUBIC (Clear, Unobstructed, Brain/Body Imaging Cocktails and Computational analysis) protocol is a recently developed tissue-clearing method that utilizes a cocktail of hydrophilic chemicals for delipidation and decolouring as well as refractive indices (RI) matching (17–19). The CUBIC-cleared samples are visualized using light-sheet fluorescent microscopy (LSFM). LSFM allows high-resolution imaging with a high acquisition speed, and thus reduces photodamage to the sample (20). The CUBIC protocol was recently introduced for a three-dimensional (3D) visualization of the entire vascular network, including all microvessels in the whole brain (21, 22).

Here, for the first time, we have extensively visualized the whole system of the brain microvessels and *Pb*ANKA parasites during ECM after CUBIC clearing. We found that *Plasmodium* parasites were accumulated in the OB significantly more than in the other parts of the brain. This comprehensive CUBIC-cleared imaging of whole brain brings attention to the OB as a critical site of parasite sequestration.

Methods

Animals and infection

C57BL/6J mice were purchased from CLEA Japan and inoculated intra-peritoneally with 1×10^6 iRBC of *Pb*ANKA [GFP (green fluorescent protein)-labelled or not, kindly provided by Prof. Yuda, Mie University (23)] as previously described (5). Peripheral blood parasitaemia was evaluated by Giemsa-stained thin blood smears on day 6 post-infection. Brains were collected for further analysis at the indicated time points.

CUBIC tissue-clearing reagents

To perform CUBIC clearing of brain, CUBIC reagents were prepared as previously described (18, 24). Briefly, CUBIC-L (10 w% *N*-butyldiethanolamine and 10 w% Triton X-100 in distilled water) (T3740, Tokyo Chemical Industry) for decolourization and delipidation, CUBIC-R (45 w% antipyrine and 30 w% nicotinamide in distilled water) (Tokyo Chemical Industry) for RI matching and CUBIC antibody-staining buffer [0.5 w% Triton X-100, 0.25 w% casein and 0.01w% sodium azide in PBS (phosphate buffered solution)] (Nacalai Tesque) were prepared.

CUBIC clearing of brains and antibody staining

Whole-brain tissue from infected and naive mice was processed according to a modified CUBIC protocol (Fig. 1A) (18). Briefly, infected mice were sampled when they displayed severe neurologically altered behaviour on day 6 or 7. Mice were anaesthetized with isoflurane and were transcardially perfused with 35 ml of ice-cold PBS followed by 30 ml of ice-cold 4% paraformaldehyde (PFA) using a Perista Pump (ATTO SJ-1211 II-H) at the maximum flow rate of 700 ml h^{-1}. The brains were immediately removed from the skull and immersed in 15 ml 4% PFA overnight at 4°C with gentle shaking at 60 rpm. The brain samples were then washed in PBS three times at room temperature (RT) for 6 h and transferred to the CUBIC-L solution for delipidation at 37°C for 5 days on a shaker at 100 rpm. CUBIC-L solution was refreshed once. After a brief washing in PBS at RT three times for more than 2 h, samples were immersed in CUBIC antibody-staining buffer containing Alexa Fluor 594-conjugated anti-α-smooth muscle actin (α-SMA, Abcam; ab202368) at 1:50 dilution for 5 days at RT on a shaker at 100 rpm. The samples were then washed with PBS, post-fixed with 1% PFA at RT for 5 h and immersed initially in 50 w% CUBIC-R (diluted with distilled water) for 5 h with shaking and then for more than 1 day in CUBIC-R for RI matching before the microscopy.

Light-sheet fluorescent microscopy

The CUBIC-treated, antibody-stained and RI-matched brain samples were immersed in an oil mixture (RI = 1.525) as previously described (18) and imaged using a custom-built light-sheet fluorescent microscope (LSFM, MVX10-LS, Olympus). A 0.63× objective lens (numerical aperture = 0.15, working distance = 87 mm) with 488 nm and 594 nm emission lasers was used to acquire the images. Images were scanned in 5–10 μm stacks in the dorsal-to-ventral direction as detailed previously (25). The acquired images were volume rendered and analysed using Imaris software.

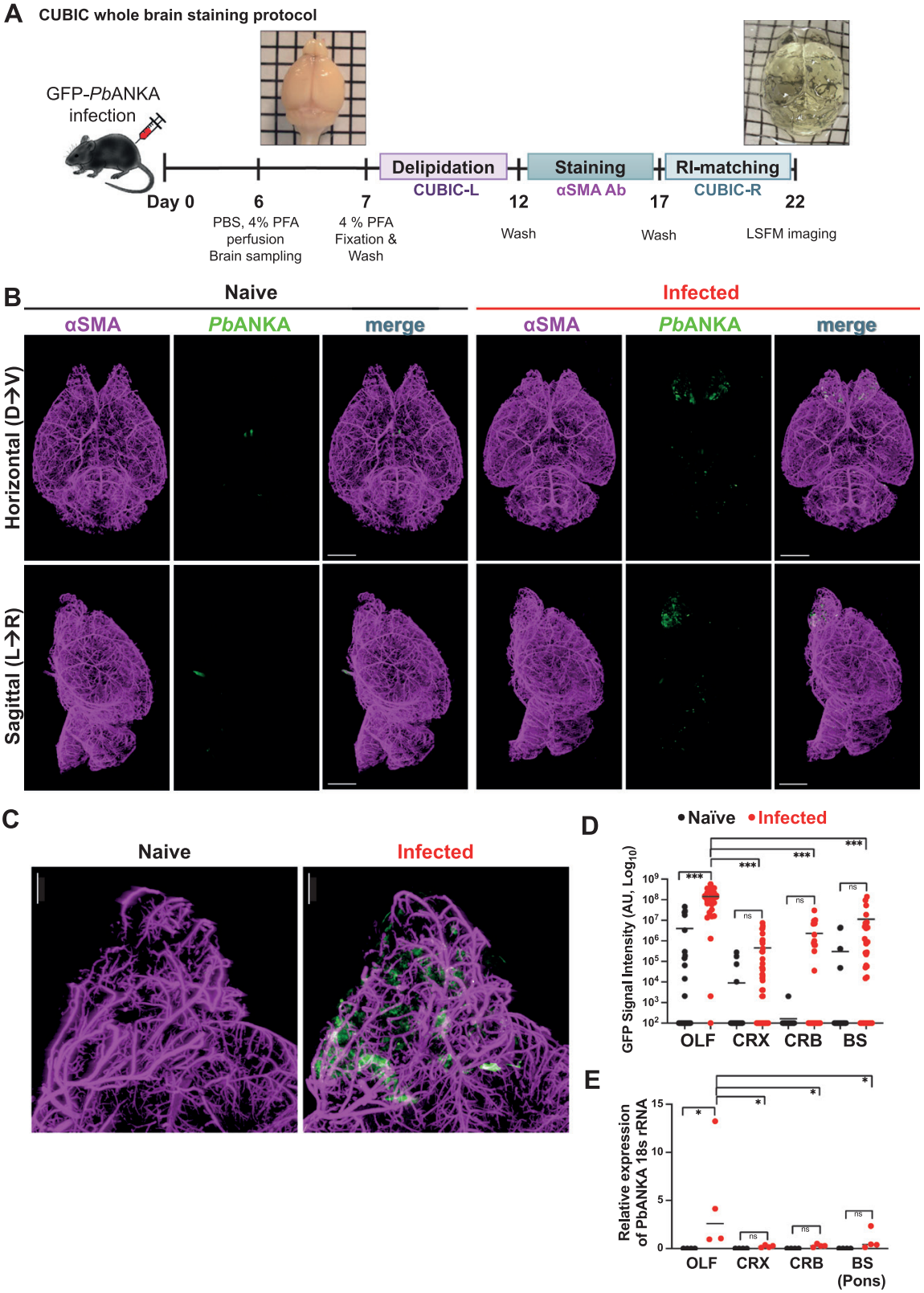

Fig. 1. Whole mouse brain imaging after CUBIC clearance reveals *Plasmodium berghei* ANKA parasite accumulation in the OB. (A) Naive and GFP-*Pb*ANKA (green)-infected mouse brains were sampled, CUBIC-treated and stained with anti-α-SMA antibody (purple), a marker of arteries and arterioles. (B) The 3D reconstituted images are shown in horizontal (dorsal-to-ventral) and sagittal (left-to-right) views. Scale bars, 3000 μm. (C) Close-up images of the OBs shown in (B) oriented in the sagittal (left-to-right) view. Scale bars, 1000 μm. (D) GFP signal intensities of four different brain regions, left and right OB, left and right cortex (CRX), cerebellum (CRB) and brainstem (BS), were approximated by creating 5–10 cubes of equal volume in each region and calculating the total GFP signal intensity in each cube ($n = 3$ mice per group). (E) Relative expression of 18S rRNA of *Pb*ANKA parasites in the OB, CRX, CRB and the brainstem (pons) by qPCR in naive and infected mice ($n = 4$ mice per group). Data are presented as the median. Statistical significance is indicated as $^{*}P < 0.05$, and $^{***}P < 0.001$ as shown by one-way ANOVA test with multiple comparisons (D) and (E).

Image analysis

Images and videos of the whole brain in the indicated orientation were generated by Imaris software (version 9.1.2; Bitplane AG, Zurich) after 3D rendering. The manual threshold for the signals was applied as needed. For the quantification of GFP signals originating from parasites in the reconstructed images, the 'Surfaces' option in Imaris was used. GFP-*Pb*ANKA isosurfaces were segmented with a smoothing surface detail of 5 μm and manual thresholding of the signal at a minimum of 2000. Comparisons between four brain regions—the OB, cerebral cortex, cerebellum and brainstem—were performed by placing 5–10 'regions of interest' of equal size (voxel size: 80 × 80 × 80, 1 voxel = 10 μm) in each region to create 5–10 independent isosurfaces per region. Isosurfaces of 5 × 2 for OB and 10 × 2 for cerebral cortex, and for a total of 10 isosurfaces for each cerebellum and brainstem were created. The total intensity sum of each of the created GFP isosurfaces was calculated as the total GFP signal intensity.

Surgical removal of the OB (olfactory bulbectomy)

Olfactory bulbectomy (OBX) in mice was performed as previously described (26). Female C57BL/6J mice were anaesthetized with ketamine and fixed on a stereotactic device (Muromachi MA-625) on a heating pad. After the eyes of the mice had been covered with petroleum jelly to prevent corneal drying, the fur on the scalp was removed with hair remover cream. An incision was made on the skull over the OB, and two holes on both sides of the bulb were drilled ~6 mm from the bregma towards the nasal bone using a micro-drill (Muromachi CMD-1000). The OBs were removed by suction via the holes with a blunted 23-gauge needle attached to a vacuum pump. The holes were then filled with bone wax (Mizuho medical innovation) and powdered with neomycin trisulfate salt hydrate (Sigma Aldrich) to prevent infection before suturing. The mice were left to heal for 2 weeks before their use in infection experiments.

Quantitative real-time reverse transcription–polymerase chain reaction analysis

Brain tissue samples from the OB, cerebral cortex, cerebellum and brainstem (pons) were sampled into TRIzol from (non-GFP-labelled) *Pb*ANKA-infected mice, 6 days post-infection, and their naive controls after transcardial perfusion with ice-cold D-PBS. The tissue samples were homogenized, the total RNA extracted and qPCR carried out for *Pb*ANKA 18s rRNA as previously described (5). The relative gene expression was calculated using the formula $2^{-\Delta CT}$ where ΔCT stands for the differential threshold cycles of *Pb*ANKA 18S rRNA gene compared with that of the mouse 18S rRNA of the same sample.

Statistical analyses

Statistical analyses were conducted using GraphPad Prism v. 9.1.0. Data are expressed as means. To analyse statistical significance, one-way ANOVA (analysis of variance) with multiple comparison was performed. The log rank (Mantel–Cox) test was performed for the analysis of survival curves. Statistical significance is represented as $^{*}P \leq 0.05$, $^{**}P \leq 0.01$ and $^{***}P \leq 0.001$.

Results and discussion

CUBIC clearing and LSFM imaging revealed that Plasmodium *parasites accumulate in the OB during ECM*

We previously demonstrated, using a combination of MRI and two-photon microscopy, that a certain part of the brain, the OB, is severely affected both anatomically and functionally during the development of ECM (5). However, MRI imaging is limited in terms of visualizing fine microvessels, and multi-photon live imaging is limited in its depth and field of view. Therefore, an analysis of deep vessel–parasite interactions at a high resolution was needed for further detail on the ECM brain. The CUBIC protocol has recently been utilized for 3D visualization of the entire vascular network, including all of the microvessels, in the whole brain (21, 24). To comprehensively visualize the deep cerebral vascular structures and brain locations with which *Plasmodium* parasites interact during ECM, mice were infected with the *P. berghei* ANKA strain expressing GFP (GFP-*Pb*ANKA) and brains from naive as well as infected mice were sampled and processed with the CUBIC reagents after transcardial perfusion with ice-cold 4% PFA (Fig. 1A). The delipidation of brains with CUBIC-L solution was followed by whole-brain immunostaining using an Alexa Flour 594-conjugated antibody against α-SMA. After RI matching with CUBIC-R solution, light-sheet microscopy (LSFM) imaging was performed. Since α-SMA is a marker for arteries and arterioles, major artery and fine arteriole structures were clearly visualized in whole brains from both the naive and infected mice (Fig. 2). Notably, GFP signals from *Pb*ANKA parasites were most evident in the OB (Fig. 1B and Fig. 2 for both the naive and infected brains). A closer look at the OB region shows that many of the GFP signals do not overlap with the α-SMA-stained vessel structure, suggesting that the parasites are found in the smallest blood vessels (i.e. the capillaries) more frequently than those stained with α-SMA or that the parasites reside in the tissues outside of the blood vessels (Fig. 1C). As mice had been extensively perfused prior to the brain sampling, the GFP-*Pb*ANKA signals in the OB suggest sequestration in the tissues, possibly because of bleeding in the olfactory capillaries. We next quantified the GFP signals in four different regions of the brain, namely the OB, cerebral cortex, cerebellum and brainstem. Compared to the other brain regions, the OB exhibited significantly higher GFP signals (Fig. 1D, $P < 0.001$). The relative expression of the *Pb*ANKA gene (18s rRNA) determined by quantitative polymerase chain reaction (PCR) confirmed that there was an increased accumulation of the parasites in the OB compared to other regions in the brain (Fig. 1E, $P < 0.05$). These CUBIC-cleared images not only reiterate the previous finding that the OB is a vulnerable site in ECM (5), but also demonstrate that the OB capillaries are the main focus of parasite accumulation. However, a caution should be noted in that there are few GFP signals coming from the brainstem, clearly less than that of the OB, which might be reflective of the late stage of ECM. We assume that the OB is affected at an earlier time point compared to the other brain regions, including the brainstem. When ECM progresses, the accumulation of parasites might expand from the OB to the other region, including the brainstem.

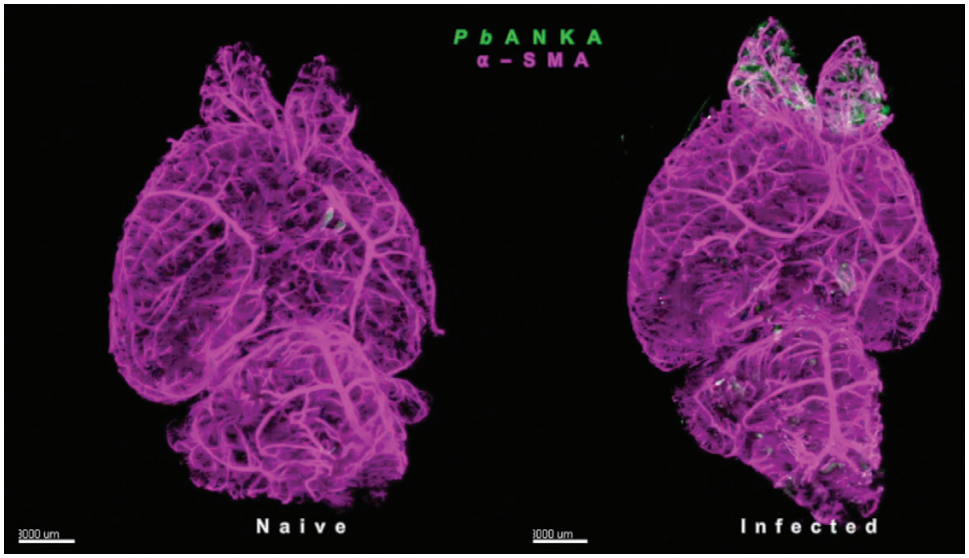

Fig. 2. Volume-rendered 3D images of naïve and GFP-*Pb*ANKA (green) infected mouse brains stained with anti-αSMA Ab (purple), after tissue clearing with CUBIC. A green fluorescent channel is included to allow comparison with the infected brain. See video online at https://academic.oup.com/intimm/advance-article-abstract/doi/10.1093/intimm/dxab060/6359340?redirectedFrom=fulltext#supplementary-data.

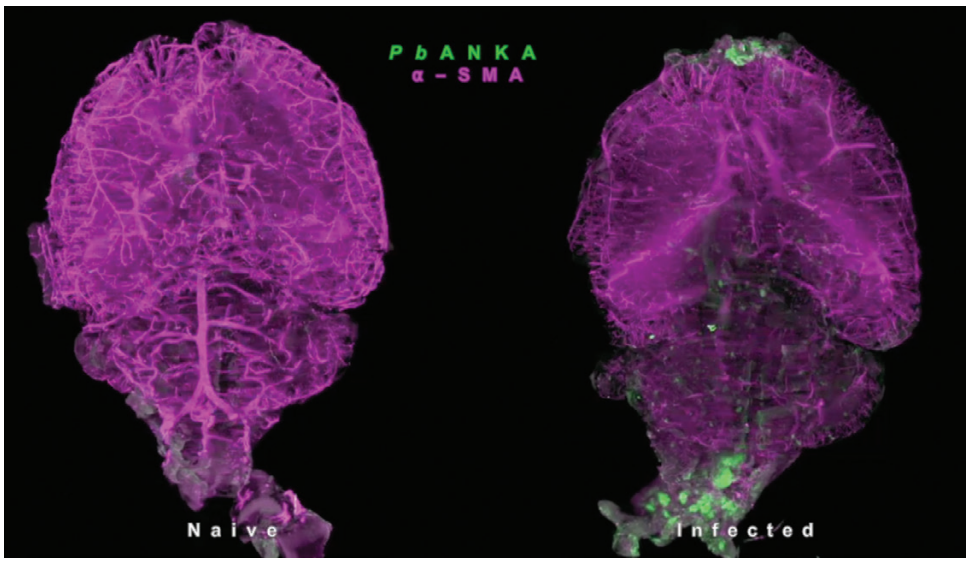

Fig. 3. Volume-rendered 3D images of bulbectomized (OBX) naïve and GFP-*Pb*ANKA (green) infected mouse brains stained with anti-αSMA Ab (purple), after tissue clearing with CUBIC. A green fluorescent channel is included to allow comparison with the infected brain. See video online at https://academic.oup.com/intimm/advance-article-abstract/doi/10.1093/intimm/dxab060/6359340?redirectedFrom=fulltext#supplementary-data.

Plasmodium *parasites accumulate in the brainstem in the absence of an OB*

The finding that the OB is the primary region of parasite localization led us to wonder whether it is required for ECM development. To gain insights into whether the OB is essential for the development of ECM, we surgically removed the OBs of the mice and then allowed them to recover for 2 weeks until the wounds healed (26), after which we infected them with GFP-*Pb*ANKA. Interestingly, 3D imaging of both the infected and naive bulbectomized (OBX) mouse brain revealed that the parasites accumulate in other locations, such as the brainstem, when the OB was removed (Fig. 3 and Fig. 4A). These areas coincide with regions that displayed obvious bleeding (Fig. 4B). Although there was no difference on day 6 of parasitaemia between the OBX and wild-type (WT) mice (10 ± 4% and 17 ± 10%, respectively; n.s. $P > 0.05$ by Mann–Whitney test), the OBX mice were found to survive slightly longer, but not significantly ($P = 0.0579$, Mantel–Cox log rank test), than their WT controls (Fig. 4C). Incomplete removal of the OBs might explain the slight difference observed in the survival of the mice. As shown in the Fig. 3 and the reconstituted image (Fig. 4A), some remnants of the bulb tissues always remained after the OBX surgery, and these regions were still affected by parasites. In fact, complete bulb removal was technically not possible, as attempts at complete removal caused immediate bleeding and death.

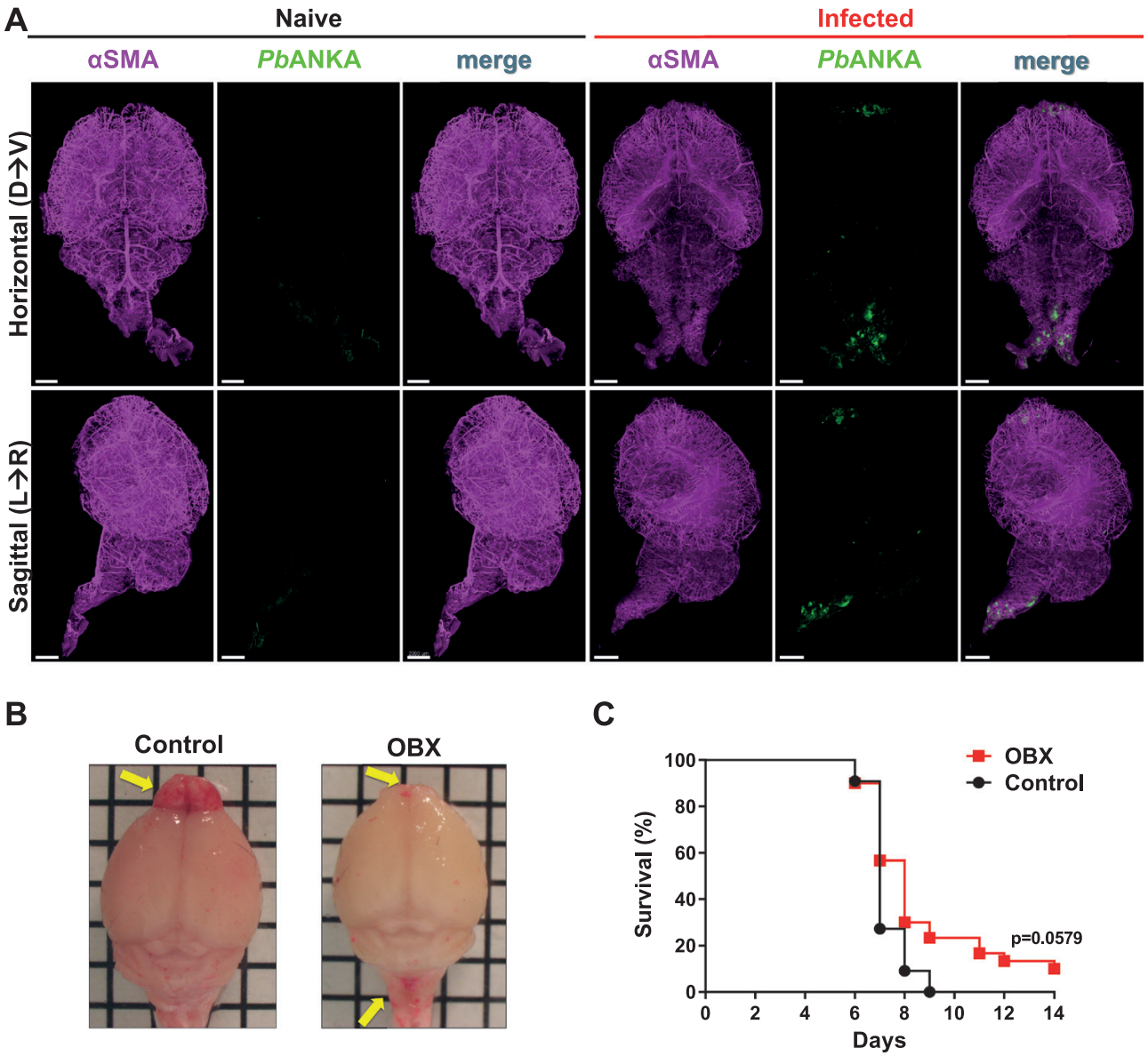

Fig. 4. Surgical removal of the OB results in the localization of *Pb*ANKA parasites in the remnants of the OB and the brainstem. (A) Bulbectomized (OBX) mice were infected with GFP-*Pb*ANKA parasites (green) and brains were sampled, CUBIC-treated and stained with anti-α-SMA antibody (purple). The 3D reconstituted images are shown in horizontal (dorsal-to-ventral) and sagittal (left-to-right) views. Scale bars, 2000 μm. (B) Dissecting microscopy images of the same control and OBX mouse brains as shown in (A). Yellow arrows indicate areas of obvious bleeding. (C) Survival curve of OBX and control mice after infection with GFP-*Pb*ANKA parasites ($P = 0.0579$ by log rank test, $n = 30$ mice for the OBX group and $n = 11$ mice for the control group).

Bilateral removal of the OBs in rodents has been commonly used as a model to investigate behavioural changes seen in patients with major depression (27). Thus, OBX in rodents reveals the mechanical disruption of neuronal connections as a model of depression. However, in our ECM model, the complete removal of blood vessels during OBX was necessary but not feasible, suggesting a limitation of the investigation which might account for the limited survival observed in the OBX mice. Notably, more parasites accumulated in the brainstem in the OBX mice, suggesting that while the parasites preferentially localize in the OB, they nevertheless accumulate elsewhere in its absence. The reason for this is currently unknown; but there are several possibilities.

Firstly, although the BBB is known to be less permissive than other blood vessels in terms of protecting the brain from harmful substances in the blood, growing evidence suggests that the blood vessels of the brain display plasticity and are immediately responsive to insults, with a great regional specificity of permissiveness. For instance, the OB and brainstem vessels are reported to be leakier than those in the cerebral cortex and cerebellum when exposed to hypoxic stress (28). Cerebral hypoxia occurs during malaria with an increase in the potential disease marker Lipocalin-2 in mice and humans (29–31); therefore, it is plausible that hypoxia in the OB contributes to the pathology in the OB (or in the brainstem, in the absence of the OB), perhaps because of the anatomical and

physiological similarities between the OB and brainstem blood vessels and/or their endothelial structures and function (9, 32).

Secondly, the OB is located on the cribriform plate over the nasal sinus, which allows complex interactions between the nerves originating from the nasal epithelium, microglia and astrocyte end-feet surrounding dense trabecular blood capillaries (3). The astrocyte and microglia sub-populations in different brain regions may have extensive molecular diversity with an array of cellular and functional properties, which may in turn correlate with various diseases (33–35). Therefore, the olfactory-specific differences in blood vessel-supporting cells such as astrocytes, pericytes and microglia may contribute to OB and brainstem bleeding, a possibility which requires further investigation.

Conclusions

Deep imaging of the entire cerebrovasculature is crucial for the evaluation and understanding of a variety of neuropathologies, including cerebral malaria, which is caused by intraerythrocytic *Plasmodium* parasites in blood vessels. By applying the newly emerged technology of the CUBIC-based tissue-clearing method, we were able to obtain high-resolution visualization of the vascular structures of the mouse brain during ECM. Genetic and fluorescent antibody-assisted labelling of blood vessels has been successfully utilized for vascular network imaging (13, 21); however, to the best of our knowledge, this study is the first to show GFP-labelled *Plasmodium* parasites inside the vessels of a soft tissue such as the brain by means of the CUBIC clearing technique. 3D whole-brain images confirmed previous MRI and two-photon live imaging findings that the OB is the first region to undergo parasite sequestration, vascular leakage and bleeding, which was also the first place for pathological $CD8^+$ T-cell accumulation (5, 36). Although not fully addressed due to technical difficulties, this bulbectomy study does afford the novel insight that in the absence of the OB, parasites localize in other brain regions, such as the brainstem. The anatomical, molecular and metabolic similarities between the OB and brainstem during ECM deserve further investigation.

The aim of several tissue-clearing techniques is to preserve proteins and/or nucleic acids and remove other components, such as lipids. After delipidation, the polarity of the solvent used for RI-matching (either in hydrophobic or hydrophilic solvent, or a hydrogel-based medium) is the most important characteristic which distinguishes the various clearing methods from each other (16). In this study we used hydrophilic solvent-based CUBIC clearing reagents that had been optimized for the mouse brain after a systematic chemical screening with a series of amino alcohols (18, 19, 22) that are easy to use in routine laboratory practice. Overall, the CUBIC clearing technique has a potential to be applied to post-mortem human brain samples (18, 37) to investigate the role of the OB in HCM which needs to be further evaluated.

Funding

This work was supported by grants from Japan Agency for Medical Research and Development (AMED J-PRIDE to K.T. (JP17fm0208023) and C.C. (17fm0208021)), and Japan Science and Technology Agency (JST-CREST (18071245) to K.J.I. and C.C.), and the International Joint Research Project of the Institute of Medical Science, the University of Tokyo (to C.C. and K.T.).

Acknowledgements

The authors wish to thank present and former Malaria Immunology Laboratory members and collaborators who greatly contributed to the research on experimental cerebral malaria pathology and imaging at Immunology Frontier Research Center (IFReC) and at the Institute of Medical Science, University of Tokyo (IMSUT). We specifically appreciate Ms Kyoko Matsuda's technical help for CUBIC clearing.

Author contributions: Conceptualization, K.T. and C.C.; Methodology and investigation, J.M.-D., M.S.J.L., K.J.I., K.T. and C.C.; Data analysis, J.M.-D., K.T. and C.C.; Writing, J.M.-D. and C.C.; Funding acquisition, K.J.I., K.T. and C.C.; Supervision, C.C. All authors have read and agreed to the final version of the manuscript.

Conflicts of interest statement: RIKEN Quantitative Biology Center has filed a patent in which K.T. is a co-inventor. The other authors declare no competing interests.

References

1 World Health Organization. 2019. *World Malaria Report 2019*. Geneva, Switzerland: World Health Organization.
2 Ghazanfari, N., Mueller, S. N. and Heath, W. R. 2018. Cerebral malaria in mouse and man. *Front. Immunol.* 9:2016.
3 Coban, C., Lee, M. S. J. and Ishii, K. J. 2018. Tissue-specific immunopathology during malaria infection. *Nat. Rev. Immunol.* 18:266.
4 Riggle, B. A., Miller, L. H. and Pierce, S. K. 2020. Desperately seeking therapies for cerebral malaria. *J. Immunol.* 204:327.
5 Zhao, H., Aoshi, T., Kawai, S. *et al.* 2014. Olfactory plays a key role in spatiotemporal pathogenesis of cerebral malaria. *Cell Host Microbe* 15:551.
6 Hoffmann, A., Pfeil, J., Alfonso, J. *et al.* 2016. Experimental cerebral malaria spreads along the rostral migratory stream. *PLoS Pathog.* 12:e1005470.
7 Dalko, E., Genete, D., Auger, F. *et al.* 2016. Heme dampens T-cell sequestration by modulating glial cell responses during rodent cerebral malaria. *Brain Behav. Immun.* 58:280.
8 Swanson, P. A., Hart, G. T., Russo, M. V. *et al.* 2016. $CD8^+$ T cells induce fatal brainstem pathology during cerebral malaria via luminal antigen-specific engagement of brain vasculature. *PLoS Pathog.* 12:e1006022.
9 Huggins, M. A., Johnson, H. L., Jin, F. *et al.* 2017. Perforin expression by CD8 T cells is sufficient to cause fatal brain edema during experimental cerebral malaria. *Infect. Immun.* 85:1.
10 Hoffmann, A., Helluy, X., Fischer, M. *et al.* 2017. *In vivo* tracking of edema development and microvascular pathology in a model of experimental cerebral malaria using magnetic resonance imaging. *J. Vis. Exp.* 2017:6.
11 Riggle, B. A., Sinharay, S., Schreiber-Stainthorp, W. *et al.* 2018. MRI demonstrates glutamine antagonist-mediated reversal of cerebral malaria pathology in mice. *Proc. Natl Acad. Sci. USA* 115:E12024.
12 Tiret, P., Chaigneau, E., Lecoq, J. *et al.* 2009. Two-photon imaging of capillary blood flow in olfactory bulb glomeruli. *Methods Mol. Biol.* 489:81.
13 Todorov, M. I., Paetzold, J. C., Schoppe, O. *et al.* 2020. Machine learning analysis of whole mouse brain vasculature. *Nat. Methods* 17:442.
14 Theer, P. and Denk, W. 2006. On the fundamental imaging-depth limit in two-photon microscopy. *J. Opt. Soc. Am. A Opt. Image Sci. Vis.* 23:3139.
15 Durr, N. J., Weisspfennig, C. T., Holfeld, B. A. *et al.* 2011. Maximum imaging depth of two-photon autofluorescence microscopy in epithelial tissues. *J. Biomed. Opt.* 16:026008.
16 Ueda, H. R., Dodt, H. U., Osten, P. *et al.* 2020. Whole-brain profiling of cells and circuits in mammals by tissue clearing and light-sheet microscopy. *Neuron* 106:369.
17 Susaki, E. A., Tainaka, K., Perrin, D. *et al.* 2015. Advanced CUBIC protocols for whole-brain and whole-body clearing and imaging. *Nat. Protoc.* 10:1709.

18 Tainaka, K., Murakami, T. C., Susaki, E. A. *et al*. 2018. Chemical landscape for tissue clearing based on hydrophilic reagents. *Cell Rep*. 24:2196.
19 Tainaka, K., Kubota, S. I., Suyama, T. Q. *et al*. 2014. Whole-body imaging with single-cell resolution by tissue decolorization. *Cell* 159:911.
20 Power, R. M. and Huisken, J. 2017. A guide to light-sheet fluorescence microscopy for multiscale imaging. *Nat. Methods* 14:360.
21 Miyawaki, T., Morikawa, S., Susaki, E. A. *et al*. 2020. Visualization and molecular characterization of whole-brain vascular networks with capillary resolution. *Nat. Commun.* 11:1104.
22 Susaki, E. A., Tainaka, K., Perrin, D. *et al*. 2014. Whole-brain imaging with single-cell resolution using chemical cocktails and computational analysis. *Cell* 157:726.
23 Ishino, T., Orito, Y., Chinzei, Y. *et al*. 2006. A calcium-dependent protein kinase regulates *Plasmodium* ookinete access to the midgut epithelial cell. *Mol. Microbiol*. 59:1175.
24 Kubota, S. I., Takahashi, K., Nishida, J. *et al*. 2017. Whole-body profiling of cancer metastasis with single-cell resolution. *Cell Rep*. 20:236.
25 Murakami, T. C., Mano, T., Saikawa, S. *et al*. 2018. A three-dimensional single-cell-resolution whole-brain atlas using CUBIC-X expansion microscopy and tissue clearing. *Nat. Neurosci*. 21:625.
26 Hendriksen, H., Korte, S. M., Olivier, B. *et al*. 2015. The olfactory bulbectomy model in mice and rat: one story or two tails? *Eur. J. Pharmacol*. 753:105.
27 Zueger, M., Urani, A., Chourbaji, S. *et al*. 2005. Olfactory bulbectomy in mice induces alterations in exploratory behavior. *Neurosci. Lett*. 374:142.
28 Halder, S. K. and Milner, R. 2020. Mild hypoxia triggers transient blood–brain barrier disruption: a fundamental protective role for microglia. *Acta Neuropathol. Commun*. 8:1.
29 Hempel, C., Combes, V., Hunt, N. H. *et al*. 2011. CNS hypoxia is more pronounced in murine cerebral than noncerebral malaria and is reversed by erythropoietin. *Am. J. Pathol.* 179:1939.
30 Coban, C., Ishii, K. J., Uematsu, S. *et al*. 2007. Pathological role of Toll-like receptor signaling in cerebral malaria. *Int. Immunol.* 19:67.
31 Sahu, P. K., Hoffmann, A., Majhi, M. *et al*. 2020. Brain magnetic resonance imaging reveals different courses of disease in pediatric and adult cerebral malaria. *Clin. Infect. Dis*. ciaa:1647.
32 Aird, W. C. 2007. Phenotypic heterogeneity of the endothelium: I. Structure, function, and mechanisms. *Circ. Res.* 100:158.
33 John Lin, C. C., Yu, K., Hatcher, A. *et al*. 2017. Identification of diverse astrocyte populations and their malignant analogs. *Nat. Neurosci*. 20:396.
34 Zeisel, A., Hochgerner, H., Lönnerberg, P. *et al*. 2018. Molecular architecture of the mouse nervous system. *Cell* 174:999.
35 De, S., Van Deren, D., Peden, E. *et al*. 2018. Two distinct ontogenies confer heterogeneity to mouse brain microglia. *Development* 145:dev152306.
36 Howland, S. W., Poh, C. M. and Rénia, L. 2015. Activated brain endothelial cells cross-present malaria antigen. *PLoS Pathog.* 11:e1004963.
37 Inoue, M., Saito, R., Kakita, A. *et al*. 2019. Rapid chemical clearing of white matter in the post-mortem human brain by 1,2-hexanediol delipidation. *Bioorg. Med. Chem. Lett*. 29:1886.